Nanoscale

PAPER

Electrically-charged recyclable graphene flakes entangled with electrospun nanofibers for the adsorption of organics for water purification†

Cite this: DOI: 10.1039/c5nr05005g

Seongpil An,[a] Hong Seok Jo,[a] Kyo Yong Song,[a] Mukund G. Mali,[a] Salem S. Al-Deyab[b] and Sam S. Yoon*[a]

Received 27th July 2015,
Accepted 15th October 2015

DOI: 10.1039/c5nr05005g

www.rsc.org/nanoscale

Graphene flakes were entrapped between nylon 6 nanofiber layers and the resulting assembly was used as a recyclable water purification membrane. Water purification was achieved *via* adsorption of the model organic pollutant (methylene blue; MB) on the surface of the graphene component. Desorption of these MB molecules was achieved by applying high voltage, which increased the removal efficiency of the recycled membrane. The adsorption and desorption mechanisms were evaluated in detail. The material characteristics of the membrane were analyzed by scanning electron microscopy, Raman, UV–visible, and Fourier transform infrared analyses.

Introduction

The difficulty in accessing clean water is an increasingly growing concern, especially in remote and drought-affected areas. The issue of accessing clean water is anticipated to become an even greater challenge[1] due to water pollution caused by the discharge of waste generated during domestic, industrial, and agricultural processes. The major pollutants in such waste include organic dyestuffs and heavy metal ions. These pollutants exert severe deleterious impacts on the health and lifestyle of human beings and the quality of the environment.[2,3] Although there are numerous water purification techniques, new and innovative methods and materials are still being sought to meet specific demands.

Carbon materials such as carbon nanotubes, graphene, and graphene oxide exhibit extraordinary electronic, thermal, and mechanical properties, and thus, they have been intensively studied.[4,5] The sp^2-hybridized single atomic layer and honeycomb structure with giant π-conjugation confer excellent electronic, thermal, and mechanical properties to graphene.[6] The theoretical surface area of graphene is 2630 $m^2\ g^{-1}$, which furnishes outstanding adsorption capacity for organics such as ethanol, methanol, protein, and DNA.[7–10] The adsorption sites provided by the large surface area expedite the adsorption of organic pollutants by graphene. The pore structure, weak polarity, and hydrophobic and lipophilic nature along with strong selective sorption capacity toward organics such as methylene blue (MB) facilitate rapid and efficient adsorption.[11] Another unique surface reactivity feature of graphene is its attraction toward organics *via* electrical force.[12] Graphene–polymer composites have been applied in various fields.[13–15] A number of adsorption properties (*i.e.* adsorption enthalpies,[7,16] adsorption energies,[8] adsorption mechanisms,[10,17] *etc.*) related with graphene have been actively studied, however, the desorption mechanisms or methods were not considerably studied compared to the adsorption case. Herein, we propose to wrap or lock graphene flakes inside tough nanofibers to achieve free inflow and outflow of water; by passing polluted water through the assembly, and toxic species or dissolved organic matter attach to the graphene surface *via* adsorption. The mass of graphene as well as the nanofiber size and amount can be controlled by varying the deposition operating conditions such as the supply voltage, nozzle-to-collector distance, precursor composition, and deposition time. In this manner, the porosity and texture of the "sandwich-like" structure membrane, comprising graphene flakes inside and nanofibers outside, can be tuned. Furthermore, we introduce a novel desorption method supplying a high voltage and demonstrate the desorption mechanism that enables the adsorption performance of the graphene to be improved even in repetitive uses.

This study presents a simple electrospinning route for the fabrication of graphene-embedded nylon nanofiber membranes on a stainless steel mesh (Fig. 1). Nylon 6 was selected as a working polymer because of its exceptional mechanical

[a]School of Mechanical Engineering, Korea University, Seoul 136-713, Republic of Korea. E-mail: skyoon@korea.ac.kr
[b]Petrochemical Research Chair, Department of Chemistry, College of Science, King Saud University, Riyadh 11451, Saudi Arabia

†Electronic supplementary information (ESI) available. See DOI: 10.1039/c5nr05005g

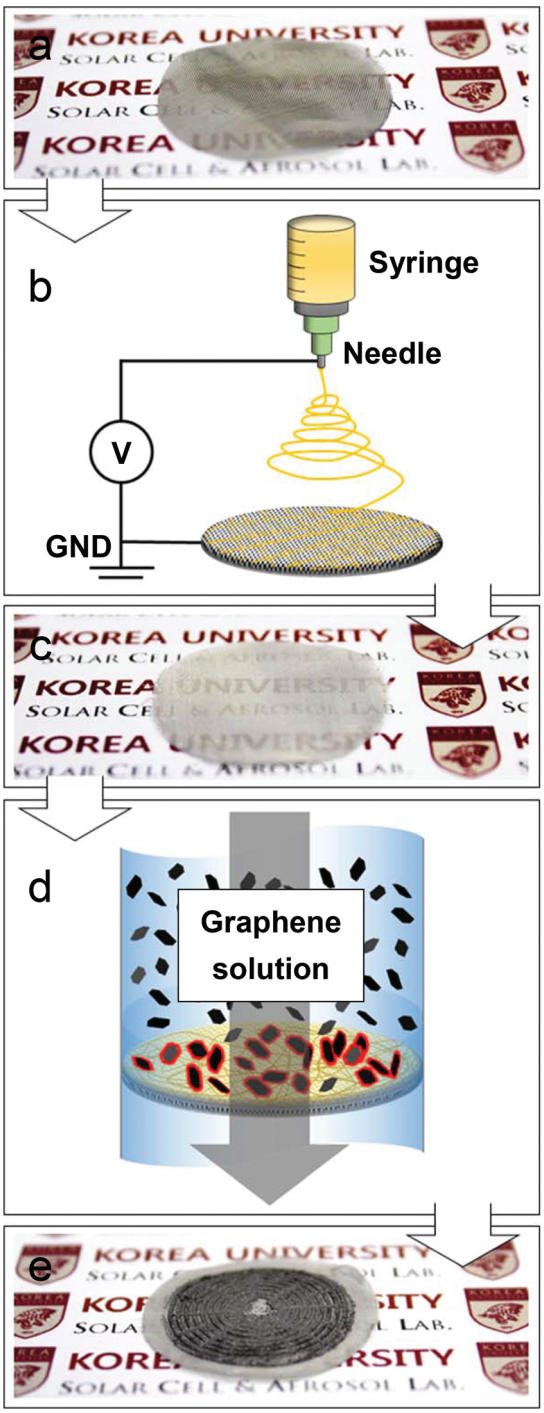

Fig. 1 The fabrication process of GNN membrane. (a) Photograph of a stainless steel 325 mesh. (b) Schematic of the electrospinning process. (c) Photograph of a nylon nanofiber-deposited steel mesh. (d) Schematic of the filtration-assisted deposition process. (e) Photograph of final GNN membrane.

strength, chemical stability, and compatibility with other materials.[18–20] The water purification capacity of this assembly is evaluated on the basis of MB decolorization.[21,22] The effect of the graphene loading and the effect of the MB flow rate and concentration on the decolorization process are discussed. The optimal operating and fabrication conditions are determined and the membrane is evaluated by subjecting the membrane to high voltage to detach the MB organics. The recyclability of the electrically regenerated membrane is also evaluated.

Experimental

Fabrication of graphene-embedded nylon nanofiber membrane

The graphene-embedded nylon nanofiber (GNN) membrane was prepared in two simple steps. Electrospinning produced nylon nanofibers were used to support graphene flakes as well as to permeate fluids as a filtration membrane. First, nylon nanofibers were electrospun onto a stainless steel 325 mesh (wire diameter = 35 μm, pore size = 43 μm), as illustrated in Fig. 1a–c. Nylon 6 (15 wt%; Sigma-Aldrich) dissolved in formic acid (Sigma-Aldrich) solution was supplied from a syringe pump (KDS, Legato 100) for 10 min at a flow rate of Q = 50 μL h^{-1} with high DC voltage of V = 12 kV at the needle (Glassman High Voltage Inc., EL40P1). The inner and outer diameters of the needle where the stable Taylor cone was formed were 0.25 and 0.52 mm, respectively (EFD, 25 gauge). In the second step, a graphene suspension containing 0.05 wt% of graphene flakes (XG Science; average diameter: 25 μm; thickness: 6–8 nm; typical surface area: 150 m^2 g^{-1}) in ethanol (Duksan Pure Chemical) was prepared. The graphene suspension was then supplied to the nanofiber-deposited steel mesh by using a syringe pump (KDS, Legato 100) at a flow rate of Q = 1 mL min^{-1} and a commercial filter holder, which has a circular-shaped structure for even distribution of graphene (Advantec MFS, Inc., Cat. no. 540100). The ethanolic graphene solution was sonicated for uniform dispersion and subsequent deposition. Graphene flakes are stacked while permeating the graphene solution through the nanofiber membrane; see Fig. 1d and e.

Characterization

The GNN membrane was characterized by using a scanning electron microscope (SEM, Hitachi, S-5000) and Fourier transform infrared spectrometer (FTIR, Horiba, LabRam Aramis IR2). The Raman shift of the membrane was measured by using a confocal Raman spectrometer (Jasco, NRS-3100) with 514 nm laser light as the excitation source. The absorbance of the aqueous MB solutions before and after treatment was monitored *via* UV–visible spectroscopy (Mecasys, OPTIZEN POP). The Brunauer–Emmett–Teller (BET) surface area was obtained by the nitrogen adsorption–desorption isotherms at 77 K (−196 °C) using a BET analyzer (Micromeritics, Tristar 3000).

Results and discussion

Graphene-embedded nylon nanofiber membrane

Fig. 2 presents an overview of the GNN membrane (center) assembly, constituent materials, and spectral characterization.

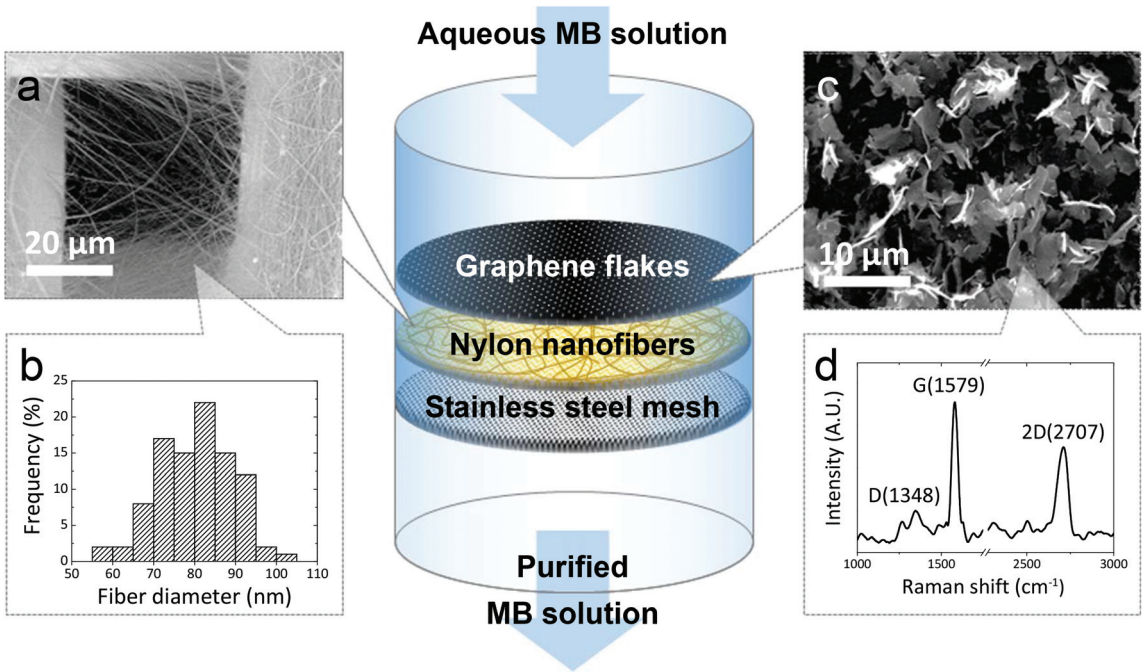

Fig. 2 Schematic of GNN membrane. (a) SEM image of nanofibers deposited on a stainless steel mesh. (b) Size distribution of nylon nanofibers. (c) SEM image of graphene flakes entrapped in the nanofiber web. (d) Raman spectrum of the membrane.

The membrane consists of a stainless steel mesh at the bottom, over which nylon nanofibers were deposited by electrospinning. Fairly dense and uniform nylon nanofibers (or webs) on the steel mesh are observed in the SEM image in the inset of Fig. 2a. The nanofibers ranged in size from 60 to 100 nm (Fig. 2b). Graphene flakes in the size range of a few to ten microns were stacked on top of the nanofibers (Fig. 2c). The model aqueous organic pollutant (MB) was passed through the membrane to purify the MB solution. The membrane was characterized *via* Raman spectroscopy, which is useful for characterization of the sp^2- and sp^3-hybridized carbon atoms of graphene (Fig. 2d). The D, 2D, and G bands of graphene appeared at 1348 cm^{-1}, 2707 cm^{-1}, and 1579 cm^{-1}, respectively. These results are in good agreement with the previously reported values for graphene.[23] The observation of these peaks confirms the presence of graphene in the membrane.

Effect of graphene loading on purification

The effect of the graphene loading on the purification capacity of the assembly was studied by evaluation of the rate of adsorption with the fixed flow rate of the MB solution (Q = 1 mL min^{-1}) and concentration (1 ppm). Prior to the investigation on the effect of the graphene loading, the adsorption capability of the nanofibers alone without graphene was first tested. No evidence of adsorption was confirmed when using the nanofibers alone, as the methylene blue solution showed no sign of purification (not shown) after passing through the nanofiber fabric. Thus, we first assured that any sign of MB purification was due to the graphene inclusion in the membranes.

The graphene loading was varied between 0.078 and 4.680 mg cm^{-2}. The samples were given an identification number (GNN#) which signifies the amount of graphene; for example, GNN5 (0.388 mg cm^{-2}) represents a five-fold increase in mass compared to GNN1 (0.078 mg cm^{-2}). The surface area of GNN1 (without the steel mesh) from BET was 123.5 m^2 g^{-1}. Given that the surface area of pristine graphene flakes and nylon fibers is 150 and 33 m^2 g^{-1}, respectively, their combined effect have resulted in reducing the overall surface area as 123.5 m^2 g^{-1}.[24] The rest of the GNN membranes with different graphene loadings had the surface area values similar to that of GNN1. This little change in the surface area indicates that the surface area is not subject to change with respect to the graphene loading. The removal efficiency was measured based on the absorption spectra with the highest peak at λ = 664 nm, which corresponds to the typical absorption wavelength of MB. The removal efficiency was defined as: $\eta = (1 - A/A_0) \times 100\%$, where A is the absorbance of purified water and A_0 is the absorbance of pure MB solution at λ = 664 nm. As shown in Fig. 3, increasing the graphene loading in the membrane produced a defined increase in the purification capacity of the GNN membrane, and complete purification was achieved with graphene loadings of GNN5 or higher. Interestingly, only a slight improvement was achieved in cases of GNN1 and GNN2 (0.155 mg cm^{-2}), whereas a substantial improvement was achieved above GNN3 (0.237 mg cm^{-2}), which indicates that there is a threshold value of the graphene loading to maximize the purification capacity.

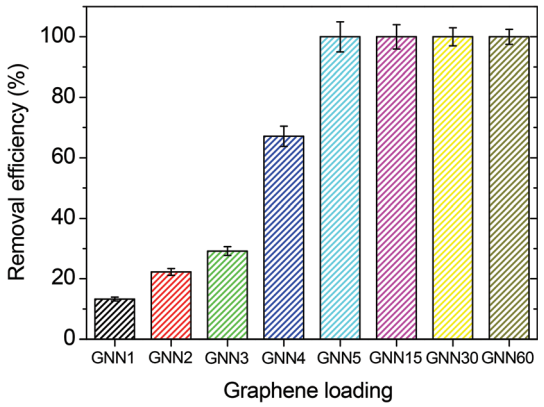

Fig. 3 Removal efficiency at different graphene loadings based on MB absorbance results. The MB solution concentration and the flow rate were fixed at 1 ppm and 1 mL min^{-1}, respectively.

Effect of MB solution flow rate on purification

It is important for a membrane to possess "high throughput" purification capability to provide a sufficient amount of purified water to fill a practical need. For this reason, the maximum flow rate beyond which purification is no longer achieved should be estimated. It is impractical to sacrifice the purification quality to achieve a high flow rate. Thus, here we refer to the maximum flow rate as the point beyond which the purification quality is no longer acceptable; quantitatively, for example, the point at which the removal efficiency is less than 90%. Fig. 4 compares the removal efficiency from using the GNN5, GNN15, and GNN30 membranes. The MB solution concentration was fixed at 1 ppm while increasing the flow rate. The complete purification (100% removal efficiency) was achieved when the flow rate was 1.0 mL min^{-1} for all graphene loadings. However, the removal efficiency dramatically reduced

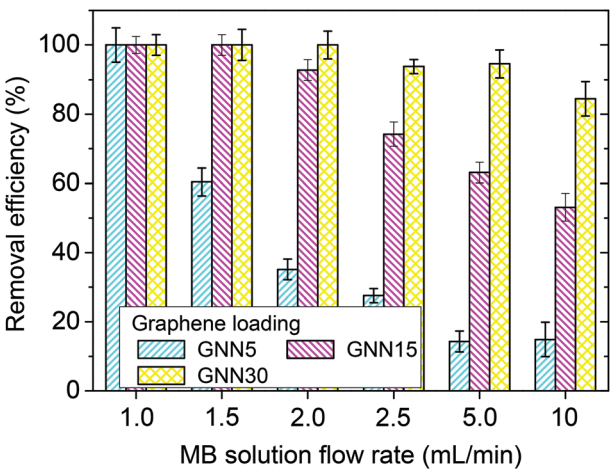

Fig. 4 Removal efficiency at different MB solution flow rates based on MB absorbance results. The MB solution concentration was fixed at 1 ppm and the graphene loadings were denoted in the graph.

for the GNN5 membrane while increasing the flow rate due to lack of graphene. The GNN15 membrane retained η = 100% up to the flow rate of 1.5 mL min^{-1}; however, η again decreased beyond 2.0 mL min^{-1}. The GNN30 membrane held η = 100% up to the flow rate of 2.0 mL min^{-1}; however, η decreased beyond 2.5 mL min^{-1}. This trend is expected and confirmed dependence of the purification capacity on the graphene loading.

Effect of MB solution concentration on purification

Fig. 5a quantitatively compares the purification capacity of the GNN5, GNN30, and GNN60 membranes while varying the concentration of the MB solution from 1 to 3 and 5 ppm. At the lowest concentration of 1 ppm, all of the membranes achieved η = 100%. However, at higher concentrations, only the GNN60 membrane achieved the removal efficiency greater than η = 90%. The overall purification capacity of the GNN membranes deteriorated at higher concentrations of MB. Upon increasing the concentration from 1 to 5 ppm for GNN5, complete purification was achieved at 1 ppm, whereas the removal efficiency was limited to 37.4% and 11.3% at 3 and 5 ppm, respectively. Even though the removal efficiency declined to below 90% in cases of GNN5 and GNN30 at 3 and 5 ppm, it should be noted that the amount of graphene used were only 1.901 and 11.47 mg, respectively (which were obtained as the product of 0.388 mg cm^{-2} × 4.9 cm^2 and 2.340 mg cm^{-2} × 4.9 cm^2) that means the developed GNN membrane showed excellent purification capability even at such a low graphene loading. Fig. 5e shows the permeability computed by the volumetric flow rate (liter per hour) divided by pressure (bar) and the cross-sectional area (m^2) of the GNN membrane, yielding the unit of L (h m^2 bar)$^{-1}$. The permeability range varies significantly depending on the graphene concentration. The permeability reduces with increasing the concentration. This trend is expected because a fluid permeating through the membrane has to experience greater drag when more graphene flakes are present, which in turn slows down the permeable capacity of the membrane, which is evidenced in Fig. 5e. Fig. 5f–h show the time series snapshots of the purification process for the GNN5, GNN30, and GNN60 membranes, respectively; also see Movie S1 in the ESI.†

The overall removal efficiency

To compare the overall purification performance of the GNN membranes as a function of both graphene loading and flow rate, the removal efficiency results are plotted on the three-dimensional axes, as shown in Fig. 6a. As expected, the GNN60 membrane yielded the best purification case. At higher flow rates, the purification capacity decreased, especially for the membranes with the low graphene loading (*i.e.*, GNN1, 2, 3, and 4). These membranes with the low graphene loadings are of no use in practice as they suffer from poor purification capability at higher flow rates. The GNN5 membrane achieved η = 100% when the flow rate was low, but the performance deteriorated upon increasing the flow rate. For the graphene loading beyond GNN15, all of the membranes performed well

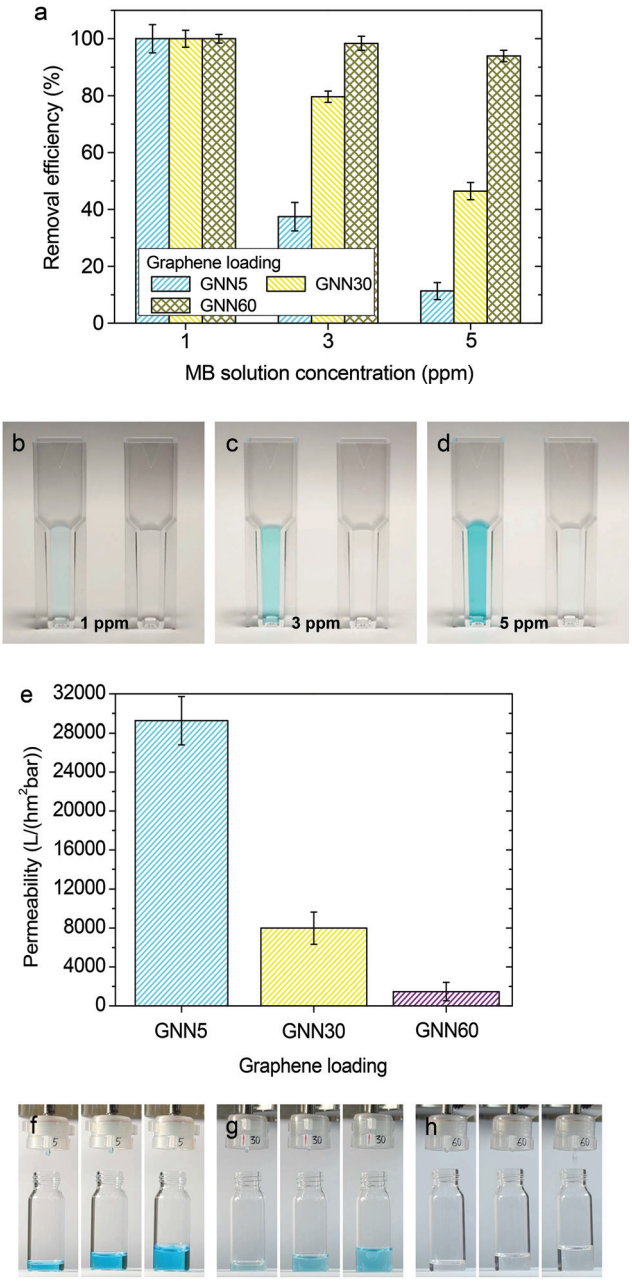

Fig. 5 (a) Removal efficiency at different MB solution concentrations based on MB absorbance results. The MB solution flow rate was fixed at 1 mL min^{-1} and the graphene loadings were denoted in the graph. Photographs of original MB solutions (left) and purified MB solutions (right) for GNN60: (b) 1 ppm, (c) 3 ppm, (d) 5 ppm. (e) Permeability of GNN5, GNN30, and GNN60 using 5 ppm MB solution. (f–h) The time series snapshots of the MB solution passing through the (f) GNN5, (g) GNN30, and (h) GNN60 membranes at t = 3, 6, 9 min, respectively.

for the wide range of flow rate. Fig. 6b quantitatively compares the removal efficiencies from various graphene loadings and MB concentrations. The results again confirmed that the higher removal efficiency was achieved when the graphene loading was higher. In addition, the purification capacity deteriorated when the concentration increased.

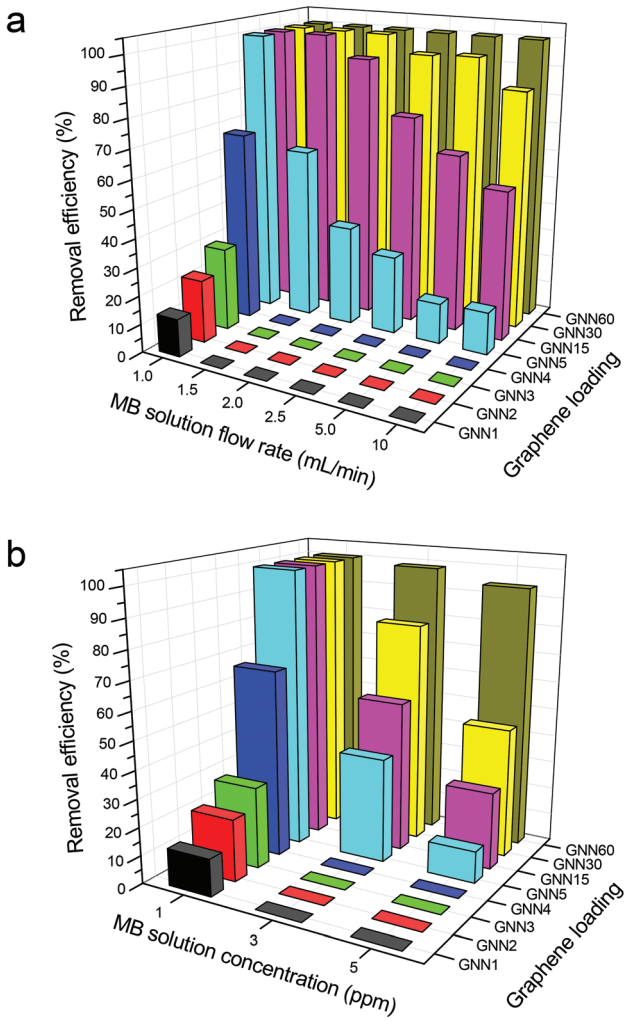

Fig. 6 Removal efficiency as a function of: (a) the graphene loading with the MB solution flow rate and (b) the graphene loading with the MB solution concentration.

Mechanism of MB adsorption on graphene

The carbon–carbon (C–C) bonds of graphene are rich in π-electrons. The most plausible type of interaction between the MB molecules and graphene is π–π stacking. The most significant interactions between MB molecules and graphene are attributed to adsorption. The MB molecules are adsorbed on the surface of the graphene sheets with an offset face-to-face orientation *via* π–π stacking interactions, during which external mass transfer between the MB solution and the graphene sheets takes place *via* boundary layer diffusion.[25]

As observed in the evaluation of the effect of graphene loading, at a lower graphene content, the removal efficiency was low. Purification (complete removal of MB) was achieved with the membrane when sufficient adsorption was accomplished due to the availability of a larger number of graphene sites. At a high graphene loading, the overall surface area of the membrane increases, which enhances the rate of adsorption of MB on graphene. On the other hand, low removal

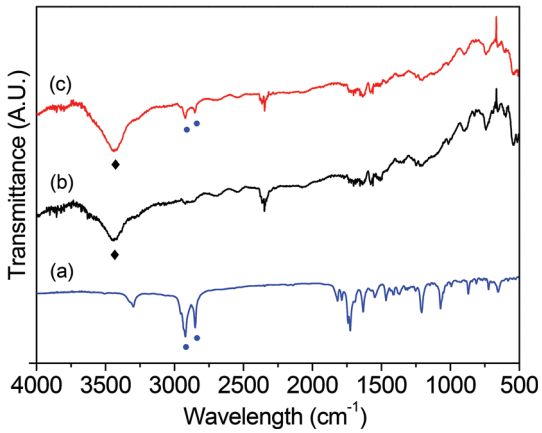

Fig. 7 FTIR spectra of (a) aqueous MB solution, (b) pristine GNN membrane, and (c) GNN membrane after treatment of MB solution.

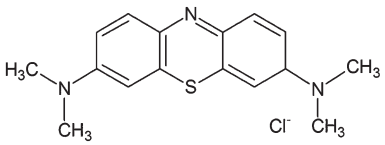

Fig. 8 Chemical structure of methylene blue.

efficiency was observed when the flow rate of the MB solution was high due to poor adsorption of the MB molecules on the graphene surface. At a high flow rate, the MB molecules have the propensity to cross the barrier membrane, leading to poor water purification as observed in Fig. 4.

To confirm the state of the MB molecules adsorbed on graphene, as-prepared GNN and the used GNN membranes were analyzed using FTIR (Fig. 7). Characteristic peaks of MB were apparent at 2920 and 2850 cm^{-1} (the bottom curve), corresponding to the stretching vibration of the C–H bonds in the methyl groups ($–CH_3$) of methylene blue (Fig. 8).[26] The middle curve in Fig. 7 shows a typical IR spectrum of pure graphene. The peak at 3446 cm^{-1} corresponds to the hydroxyl (O–H) groups. The peaks observed in the region of 1500–1800 cm^{-1} are ascribed to the carbonyl and carboxyl groups on the surface of graphene.[27] In the used GNN membranes, the top curve shows peaks corresponding to MB as well as graphene, which confirms the adsorption of MB on graphene.

Recyclability

In general, the filtration capacity of a filter declines with repetitive use given that the filter (in this case, the graphene sheet) can only hold a certain amount of adsorbate (*i.e.*, MB molecules); that is, the adsorption site or area is limited. In contrast with the rapid adsorption of organic pollutants by graphene, the desorption process is quite a challenge because of strong bonding between graphene and the attached organic pollutants (MB molecules in this study).[12]

Herein, attempts were made to desorb the MB molecules from graphene by applying 10 kV of high voltage (HV) for 1 min prior to the start of every cycle. Fig. 9 shows the results of the recyclability test performed with (red) and without (black) HV treatment of the used GNN5 membranes. After a few cycles, the MB removal capacity of the membrane not subjected to (without) HV treatment declined substantially, reaching below 40% removal efficiency at the fifth cycle. However, HV treatment of the used membrane resulted in an enhancement of the removal efficiency with repetitive use (right column, red data bars in Fig. 9a). This improvement was repeatedly confirmed for all cycle numbers. Therefore, desorption of MB molecules from graphene was successfully achieved, as confirmed through this recyclability test.

Graphene is well known for its significant conductivity (electron mobility at room temperature = 250 000 $cm^2\ V^{-1}\ s^{-1}$) owing to its zero band gap. This property of graphene plays a significant role during the HV treatment for the desorption of MB molecules from graphene. Rahaman *et al.* investigated the electrostatic interaction between viral particles and multi-walled carbon nanotubes under application of an external electric field.[28] They observed inactivation of the adsorbed viral particles by surficial oxidation. In the present study, HV treatment effectively broke the bond between the MB molecules and graphene *via* oxidation/decomposition (Fig. 9b). The mechanism of MB oxidation at the graphene surface owing to the HV treatment can be explained as follows:

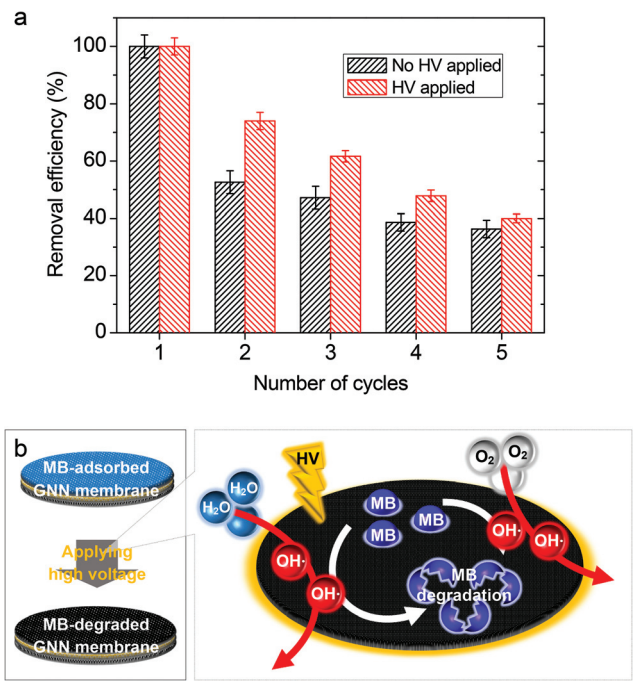

Fig. 9 (a) Removal efficiency of GNN5 membrane over multiple cycles for the membrane subjected to high voltage (HV) and not subjected to HV treatment. The MB solution concentration and the flow rate were fixed at 1 ppm and 1 mL min^{-1}, respectively. (b) Schematic of the MB degradation process.

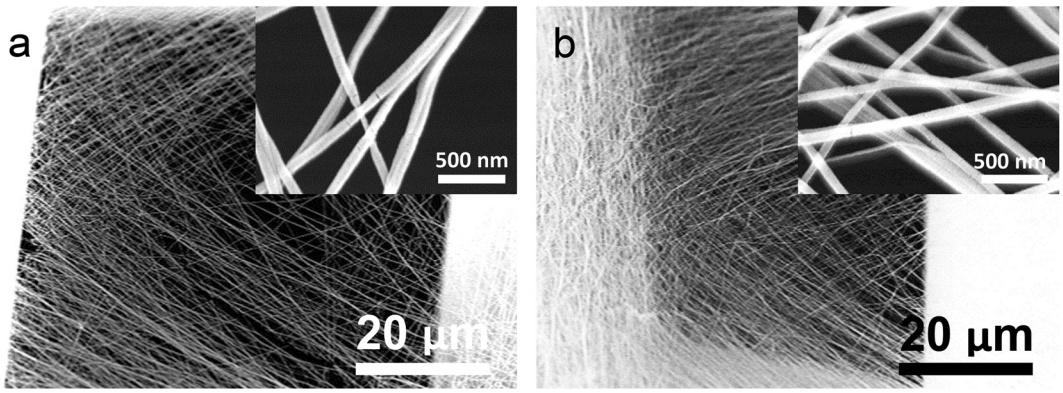

Fig. 10 SEM images of (a) as-deposited and (b) HV-treated nylon nanofibers on the steel mesh.

Hydroxyl radicals are generated by the following reactions:

$$e^-_{(HV)} + H_2O \rightarrow H^\bullet + OH^\bullet + e^- (OH^\bullet \text{ radical generation}) \quad (1)$$

$$e^-_{(HV)} + H_2O \rightarrow H_2O^+ + 2e^- (H_2O^+ \text{ ion formation}) \quad (2)$$

$$H_2O^+ + H_2O \rightarrow H_3O^+ + OH^\bullet \ (OH^\bullet \text{ radical generation}) \quad (3)$$

In addition to generation from the decomposition of water, hydroxyl radicals can also be generated by electronically excited oxygen atoms ($O(^1D)$) from oxygen (O_2) in the air as follows:[29]

$$e^-_{(HV)} + O_{2(g)} \rightarrow O(^1D) + O(^3P) + e^- (\text{O atom formation}) \quad (4)$$

$$O(^1D) + H_2O \rightarrow OH^\bullet + OH^\bullet \ (OH^\bullet \text{ radical generation}) \quad (5)$$

These generated hydroxyl radicals are responsible for the degradation and consequent removal of MB from the graphene surface as follows:

$$C_{16}H_{18}N_3SCl + OH^\bullet \rightarrow C_{16}H_{18}N_3SCl(OH) \quad (6)$$

$$C_{16}H_{18}N_3SCl(OH) + OH^\bullet \rightarrow C_{16}H_{18}N_3SCl(OH)_2 \quad (7)$$

$$C_{16}H_{18}N_3SCl(OH)_2 + OH^\bullet \rightarrow C_{16}H_{18}N_3SCl(OH)_3 \quad (8)$$

$$C_{16}H_{18}N_3SCl(OH)_3 \rightarrow \text{Decomposition products (amines, nitrates, } CO_2\text{, } etc.) \quad (9)$$

The $OH^\bullet$ radicals react with MB molecules to initially form hydroxide species that are later decomposed into amines, nitrates, CO_2, *etc.*, as shown in eqn (6)–(9). The decomposition of adsorbed MB molecules in the first cycle makes more area on the surface of graphene available, providing more binding sites for the MB molecules in the second cycle. This effect is evidenced by the improved water purification performance (*i.e.*, MB removal capacity) of the present GNN membranes. A comparison of the as-prepared nanofibers on the stainless steel mesh and those subjected to the HV treatment is presented based on SEM analysis (Fig. 10). No sign of degradation of the nanofibers was apparent even after the HV treatment. Thus, in theory, this membrane can be recycled indefinitely as long as the nanofibers remain mechanically and electrically resistant to the HV treatment, which is the case here.

Conclusion

A water purification membrane was fabricated by entrapping graphene flakes between nylon nanofiber layers. The fabricated membrane was found to be effective for water purification based on the removal of the model pollutant, methylene blue. The removal efficiency varied as a function of the amount of pollutant passing through the membrane. Evaluation of the effect of the graphene loading on the purification performance showed that there is a threshold value (0.237 mg cm^{-2}) of the graphene loading to maximize the purification capacity of the membrane. Removal of the model pollutant by the membrane occurs *via* adsorption of the MB molecules on the surface of the graphene flakes. The adsorption phenomenon was confirmed by FTIR. Furthermore, electrically driven desorption was applied as a novel approach for recycling the used membrane. Applying high voltage to the membrane was effective for desorbing the MB molecules without sacrificing the mechanical stability of the nanofibers that entrap the graphene flakes.

Acknowledgements

This research was supported by National Research Foundation (NRF-2013M3A6B1078879) and NRF-2013R1A2A2A05005589. This research was also supported by a Special International Collaboration Grant provided by Korea University. The authors also extend their appreciation to the Deanship of Scientific Research at King Saud University for funding this Prolific Research group (PRG-1436-03).

References

1 M. A. Shannon, P. W. Bohn, M. Elimelech, J. G. Georgiadis, B. J. Marinas and A. M. Mayes, *Nature*, 2008, **452**, 301–310.
2 T. S. Sreeprasad, S. M. Maliyekkal, K. P. Lisha and T. Pradeep, *J. Hazard. Mater.*, 2011, **186**, 921–931.
3 Z. Sui, Q. Meng, X. Zhang, R. Mab and B. Caob, *J. Mater. Chem.*, 2012, **22**, 8767–8771.

4 W. Yang, K. R. Ratinac, S. P. Ringer, P. Thordarson, J. J. Gooding and F. Braet, *Angew. Chem., Int. Ed.*, 2010, **49**, 2114–2138.

5 S. H. Lee, D. H. Lee, W. J. Lee and S. O. Kim, *Adv. Funct. Mater.*, 2011, **21**, 1338–1354.

6 Y. Zhang and C. Pan, *J. Mater. Sci.*, 2010, **46**, 2622–2626.

7 P. Lazar, F. e. Karlický, P. Jurečka, M. s. Kocman, E. Otyepková, K. r. Šafářová and M. Otyepka, *J. Am. Chem. Soc.*, 2013, **135**, 6372–6377.

8 E. Schröder, *J. Nanomater.*, 2013, **2013**.

9 C. J. Russo and L. A. Passmore, *Nat. Methods*, 2014, **11**, 649–652.

10 J. S. Park, N.-I. Goo and D.-E. Kim, *Langmuir*, 2014, **30**, 12587–12595.

11 M. Zhao and P. Liu, *Desalination*, 2009, **249**, 331–336.

12 W. Zhang, C. Zhou, W. Zhou, A. Lei, Q. Zhang, Q. Wan and B. Zou, *Bull. Environ. Contam. Toxicol.*, 2011, **87**, 86–90.

13 Q. Bao, H. Zhang, J.-x. Yang, S. Wang, D. Y. Tang, R. Jose, S. Ramakrishna, C. T. Lim and K. P. Loh, *Adv. Funct. Mater.*, 2010, **20**, 782–791.

14 J. L. Vickery, A. J. Patil and S. Mann, *Adv. Mater.*, 2009, **21**, 2180–2184.

15 S. Villar-Rodil, J. I. Paredes, A. Martínez-Alonso and J. M. D. Tascón, *J. Mater. Chem.*, 2009, **19**, 3591.

16 F. Karlicky, E. Otyepková, P. Banáš, P. Lazar, M. Kocman and M. Otyepka, *J. Phys. Chem. C*, 2015.

17 Y. Li, Q. Du, T. Liu, X. Peng, J. Wang, J. Sun, Y. Wang, S. Wu, Z. Wang and Y. Xia, *Chem. Eng. Res. Des.*, 2013, **91**, 361–368.

18 H. R. Pant, M. P. Bajgai, K. T. Nam, K. H. Chu, S.-J. Park and H. Y. Kim, *Mater. Lett.*, 2010, **64**, 2087–2090.

19 H. R. Pant, M. P. Bajgai, K. T. Nam, Y. A. Seo, D. R. Pandeya, S. T. Hong and H. Y. Kim, *J. Hazard. Mater.*, 2011, **185**, 124–130.

20 E. S. Medeiros, G. M. Glenn, A. P. Klamczynski, W. J. Orts and L. H. C. Mattoso, *J. Appl. Polym. Sci.*, 2009, **113**, 2322–2330.

21 J.-J. Park, J.-G. Lee, D.-Y. Kim, J.-H. Hong, J.-J. Kim, S. Hong and S. S. Yoon, *Environ. Sci. Technol.*, 2012, **46**, 12510–12518.

22 S. An, M. W. Lee, B. N. Joshi, A. Jo, J. Jung and S. S. Yoon, *Ceram. Int.*, 2014, **40**, 3305–3313.

23 A. C. Ferrari, *Solid State Commun.*, 2007, **143**, 47–57.

24 Y. J. Ryu, H. Y. Kim, K. H. Lee, H. C. Park and D. R. Lee, *Eur. Polym. J.*, 2003, **39**, 1883–1889.

25 H. Yoon, S. H. Na, J. Y. Choi, S. S. Latthe, M. T. Swihart, S. S. Al-Deyab and S. S. Yoon, *Langmuir*, 2014, **30**, 11761–11769.

26 O. V. Ovchinnikov, S. V. Chernykh, M. S. Smirnov, D. V. Alpatova, R. P. Vorob'eva, A. N. Latyshev, A. B. Evlev, A. N. Utekhin and a. A. N. Lukin, *J. Appl. Spectrosc.*, 2007, **74**, 809–816.

27 H. Li, T. Lu, L. Pan, Y. Zhang and Z. Sun, *J. Mater. Chem.*, 2009, **19**, 6773.

28 M. S. Rahaman, C. D. Vecitis and M. Elimelech, *Environ. Sci. Technol.*, 2012, **46**, 1556–1564.

29 P. Lukes and B. R. Locke, *J. Phys. D: Appl. Phys.*, 2005, **38**, 4074.